Research Article | Vol. 27, No. 8 | 15 Apr 2019 | OPTICS EXPRESS 11370
Optics EXPRESS

Super chirped rogue waves in optical fibers

SHIHUA CHEN,[1,*] YI ZHOU,[1] LILI BU,[1] FABIO BARONIO,[2] JOSE M. SOTO-CRESPO,[3,5] AND DUMITRU MIHALACHE[4]

[1]School of Physics, Southeast University, Nanjing 211189, China
[2]INO CNR and Dipartimento di Ingegneria dell'Informazione, Università di Brescia, Via Branze 38, 25123 Brescia, Italy
[3]Instituto de Óptica, Consejo Superior de Investigaciones Científicas, Serrano 121, Madrid 28006, Spain
[4]Horia Hulubei National Institute for Physics and Nuclear Engineering, Department of Theoretical Physics, Magurele-Bucharest RO-077125, Romania
[5]j.soto@csic.es
[*]cshua@seu.edu.cn

Abstract: The super rogue wave dynamics in optical fibers are investigated within the framework of a generalized nonlinear Schrödinger equation containing group-velocity dispersion, Kerr and quintic nonlinearity, and self-steepening effect. In terms of the explicit rogue wave solutions up to the third order, we show that, for a rogue wave solution of order n, it can be shaped up as a single super rogue wave state with its peak amplitude $2n + 1$ times the background level, which results from the superposition of $n(n + 1)/2$ Peregrine solitons. Particularly, we demonstrate that these super rogue waves involve a frequency chirp that is also localized in both time and space. The robustness of the super chirped rogue waves against white-noise perturbations as well as the possibility of generating them in a turbulent field is numerically confirmed, which anticipates their accessibility to experimental observation.

1. Introduction

As an optical counterpart of the infamous oceanic rogue waves that have been held responsible for numerous marine misfortunes [1], optical rogue waves [2] are attracting burgeoning interest of research on both theoretical and experimental sides [3, 4], due to their potential applications and their comparative ease to create and capture in a laboratorial environment [5]. They are associated with solitons [6–10], as both of them can be generated through a process known as modulation instability (MI) [11]. However, while solitons are stationary wavepackets that can propagate in a dispersive medium with no distortion, rogue waves are transient ones that are localized in both time and space, hence seeming to appear from nowhere and disappear without a trace [12]. Despite their unpredictability, rogue waves have now been successfully observed in a number of optical settings such as optical fibers [13], mode-locked lasers [14], microresonators [15], and photorefractive ferroelectrics [16], not to mention those observed in filamentation [17], beam speckles [18], caustics [19], and integrable turbulence [20].

On mathematical aspect, the rogue wave concept is generally thought of as a rational polynomial construct based on the integrability of a class of nonlinear differential equations [21]. A typical example is the Peregrine soliton, which was first discovered in 1983 by Peregrine as the fundamental rational solution to the celebrated nonlinear Schrödinger (NLS) equation [22]. It is built on a finite continuous background, reaching a climax three times the background height followed by two deep troughs, and is therefore not a genuine 'soliton'. As it can mimic realistic extreme wave events, the Peregrine soliton has become a popular prototype of rogue waves in many areas [5, 23]. Recent studies reveal that Peregrine solitons are universal solutions of majority of integrable models [24–26], not peculiar to the NLS equation, and have many interesting variants of emergence such as dark Peregrine solitons [27], anomalous Peregrine solitons [28], and chirped Peregrine solitons [29]. Of particular interest is the chirped Peregrine

#357873 https://doi.org/10.1364/OE.27.011370
Journal © 2019 Received 17 Jan 2019; revised 27 Mar 2019; accepted 27 Mar 2019; published 9 Apr 2019

soliton, which can possess an extra doubly localized chirp while keeping the intensity features of the original Peregrine soliton. Such chirped version of Peregrine solitons can be reminiscent of the well-established chirped soliton concept [30, 31] that has been used for many practical purposes (e.g., compression [32], amplification [33], communication [34], etc.).

In the past decade, intriguing rogue wave dynamics of higher hierarchy were also explored, which can be classified into two categories: super rogue waves and multi-rogue waves. While the multi-rogue wave, as its name implies, is a combination of multiple well-separated Peregrine solitons [35, 36], by the super rogue wave [37] we mean a rogue wave whose intensity takes its maximum allowable value and is much stronger than that of Peregrine solitons. Typical experiments include those carried out by Chabchoub *et al.* who observed the super hydrodynamical rogue waves in a water-wave tank [37], and by Baronio *et al.* who observed vector dark 'three sisters' in a telecommunication fiber [38], to name a few. No doubt, the success of these experimental observations justifies the quest of higher-order rogue wave solutions [39–41].

In this article, we investigate the chirped version of higher-order rogue waves, termed super chirped rogue waves for their super high peak amplitude, within the framework of a generalized NLS equation that contains the group-velocity dispersion (GVD), the Kerr and quintic nonlinearity, and the self-steepening effect [42]. Such kind of generalized NLS equation, with different reductions, usually applies to the description of ultrashort pulse propagation in optical fibers [43, 44] and also to the description of high-intensity pulse propagation [45], controllable self-steepening [46, 47], and generation of Cherenkov radiation [48] in quadratic crystals. In terms of the explicit rogue wave solutions up to the third order, we show that, for a rogue wave solution of order n, it can be shaped up as a single super rogue wave state with its peak amplitude $2n + 1$ times the background level, which arises from the superposition of $n(n + 1)/2$ Peregrine solitons. In particular, we reveal that these super rogue waves involve a frequency chirp that is also localized in both time and space. The stability of the super chirped rogue waves as well as the possibility to generate them in a turbulent field is numerically confirmed, which anticipates an accessibility to experimental observation.

2. Theoretical framework

The propagation of ultrashort pulses in a single-mode optical fiber can be modelled by the dimensionless cubic-quintic (CQ) NLS equation [42]:

$$iE_z + \frac{1}{2}E_{tt} + \sigma|E|^2E + i\gamma(|E|^2E)_t + i(\mu - 2\gamma)(|E|^2)_tE + \frac{1}{2}(\mu - \gamma)(\mu - 2\gamma)|E|^4E = 0, \tag{1}$$

where $E(z, t)$ is the normalized complex envelope of an optical pulse, and z and t are the distance and retarded time, respectively. Subscripts z and t stand for partial derivatives. While the constant coefficient $\frac{1}{2}$ points to the GVD effect, the coefficient σ denotes the Kerr nonlinearity, γ accounts for the pulse self-steepening effect (we assume $\gamma \geqslant 0$ without loss of generality) [46, 47], and μ relates to the nonlinearity dispersion, which can result in self-frequency shift if μ is complex [43], and to the quintic nonlinearity, which was often found in highly nonlinear materials such as chalcogenide fibers [44]. In cases of self-focusing, self-defocusing, and zero Kerr nonlinearities, σ can be normalized to 1, -1, and 0. In the context of fiber optics, the term $|E|^2E$ in Eq. (1) is often referred to as self-phase modulation (which is actually a temporal analog of self-focusing), and then the coefficient σ can be scaled out to the GVD term, which will be termed anomalous dispersion if $\sigma > 0$ and normal dispersion if $\sigma < 0$ [6, 44]. It is worth noting that, to attain integrability [42], the last three terms on the left hand side of Eq. (1) have been related by two real free parameters γ and μ. Besides, in order to weigh the nonlinearity factors that affect the chirped rogue wave dynamics, we have excluded the higher-order dispersion terms from Eq. (1),

which usually appear in the high NLS equation hierarchy [49].

As one might expect, Eq. (1) is rather general, as it can reduce to a series of well-established integrable equations such as the celebrated NLS equation ($\mu = \gamma = 0$), the Chen–Lee–Liu type NLS (CLL–NLS) equation ($\mu = \gamma \neq 0$) [50], the Kaup–Newell type NLS (KN–NLS) equation ($\mu = 2\gamma$) [51], the Gerdjikov–Ivanov (GI) equation ($\mu = 0$) [52], and the Kundu–Eckhaus (KE) equation ($\gamma = 0$) [53, 54]. The fundamental rational solution, termed chirped Peregrine soliton, of this equation has been obtained by a gauge transformation method [29]. It naturally generalizes previous fundamental solutions found for the above reduced equations [39, 55–58]. In this work, we present for the first time, to the best of our knowledge, the nth-order rogue wave solution of Eq. (1), and particularly its explicit solution forms up to the third order, using a nonrecursive Darboux transformation method [59].

It is easy to show that this general integrable equation is equivalent to the compatibility of the following Lax pair of the linear eigenvalue problem

$$\mathbf{R}_t = \mathbf{U}\mathbf{R}, \qquad \mathbf{R}_z = \mathbf{V}\mathbf{R}, \tag{2}$$

where $\mathbf{R} = [r(z,t,\lambda), s(z,t,\lambda)]^T$ (T means a matrix transpose), and

$$\begin{aligned}
\mathbf{U} &= -\frac{i(\lambda-\sigma)\sigma_3}{2\gamma} + \sqrt{\lambda}\mathbf{Q} + \frac{i(\mu-2\gamma)}{2}\sigma_3\mathbf{Q}^2, \\
\mathbf{V} &= -\frac{i(\lambda-\sigma)^2\sigma_3}{4\gamma^2} + \frac{\sqrt{\lambda}}{2}\left(\frac{\lambda-\sigma}{\gamma}\mathbf{Q} - i\sqrt{\lambda}\sigma_3\mathbf{Q}^2 + \mu\mathbf{Q}^3 + i\sigma_3\mathbf{Q}_t\right) \\
&\quad + \frac{\mu-2\gamma}{4}\left[i(2\mu-\gamma)\sigma_3\mathbf{Q}^4 + (\mathbf{Q}\mathbf{Q}_t - \mathbf{Q}_t\mathbf{Q})\right],
\end{aligned} \tag{3}$$

with λ being the free spectral parameter, $\sigma_3 = \mathrm{diag}(1,-1)$, and

$$\mathbf{Q} = \begin{bmatrix} 0 & E(z,t) \\ -E^*(z,t) & 0 \end{bmatrix}.$$

The asterisk over the field variables signifies the complex conjugate and 'diag' means a diagonal matrix. For our present purpose, we consider the plane-wave solution of Eq. (1) as an initial potential, which can be defined by its amplitude (a), wavenumber (k), and frequency (ω) through

$$E_0 = a\exp[i(kz + \omega t)], \tag{4}$$

under the dispersion relation

$$k = \eta a^2 + \frac{1}{2}(\mu-\gamma)(\mu-2\gamma)a^4 - \frac{\omega^2}{2}, \quad (\text{here } \eta = \sigma - \gamma\omega). \tag{5}$$

With this plane-wave potential, the linear eigenvalue problem (2) can be readily solved to obtain

$$\mathbf{R}(\lambda) = \mathbf{G}(\Gamma_1\mathbf{N}_1 + \Gamma_2\mathbf{N}_2), \tag{6}$$

where Γ_j ($j = 1, 2$, the same below) are arbitrary complex constants, $\mathbf{G} = \mathrm{diag}(1, E_0^*/a)$, and

$$\mathbf{N}_j = \begin{bmatrix} 1 \\ \frac{i[a^2\gamma(\mu-2\gamma)+2\gamma\phi_j+\lambda-\sigma]}{2a\gamma\sqrt{\lambda}} \end{bmatrix} \exp\left[i(\theta_j z + \phi_j t)\right], \tag{7}$$

with

$$\phi_j = \frac{\omega}{2} - \frac{(-1)^j}{2\gamma}\sqrt{(\lambda + a^2\gamma^2 - \beta^2/a^2)^2 + 4\beta^2\gamma^2}, \tag{8}$$

Optics EXPRESS

$$\theta_j = \frac{k}{2} + \frac{\omega - 2\phi_j}{4\gamma}[a^2\gamma(2\mu - \gamma) + 2\omega\gamma + \beta^2/a^2 - \lambda], \tag{9}$$

$$\beta = a\sqrt{\eta - a^2\gamma(\mu - \gamma)}. \tag{10}$$

An inspection of Eqs. (8) and (9) reveals that, if $\lambda = (\beta/a + i\gamma a)^2 \equiv \lambda_0$, there will be $\phi_1 = \phi_2 = \phi_0$ and $\theta_1 = \theta_2 = \theta_0$, where

$$\phi_0 = \frac{\omega}{2}, \quad \theta_0 = \frac{k}{2}. \tag{11}$$

This implies further that $\mathbf{N}_1 = \mathbf{N}_2$. Then, by choosing appropriate parameters $\Gamma_{1,2}$ in Eq. (6), the ratio of the entry r of the column vector $\mathbf{R}$ to the other one s could have a simple rational form (excluding the plane-wave exponential factor), which, according to the Darboux dressing formalism, results in the rogue wave solutions of Eq. (1) [60,61]. On the other hand, as is evident below, λ_0 must be complex, or equivalently, β must be real, which gives the parameter condition for existence of a rogue wave:

$$\omega < \sigma/\gamma - a^2(\mu - \gamma). \tag{12}$$

This condition is the same as that obtained using the theory of baseband MI [3,62,63] and suggests that rogue waves can exist in both the self-focusing (or equivalently, anomalous dispersion) and the defocusing (normal dispersion) regimes, when the self-steepening effect, denoted by the parameter γ, comes into play [29,61].

As employed in [59], there is a more convenient way to obtain the rogue wave solutions. To this end, one can let

$$\lambda = \lambda_0 + \chi\epsilon^2, \quad \chi = \lambda_0 - \lambda_0^* = 4i\beta\gamma, \tag{13}$$

where ϵ is a complex perturbation parameter, and let the parameters $\Gamma_{1,2}$ be

$$\Gamma_1 = \frac{1}{2}\sum_{j=1}^{n}\left(\gamma_{2j-1} + \frac{\gamma_{2j}}{\epsilon}\right)\epsilon^{2(j-1)}, \quad \Gamma_2 = \frac{1}{2}\sum_{j=1}^{n}\left(\gamma_{2j-1} - \frac{\gamma_{2j}}{\epsilon}\right)\epsilon^{2(j-1)}, \tag{14}$$

where γ_j ($j = 1, 2, \cdots, 2n$) are arbitrary complex constants (which should not be confused with the system parameter γ). Then, the factorized eigenvector $\Theta(\lambda) = \mathbf{G}^{-1}\mathbf{R}(\lambda) = \Gamma_1\mathbf{N}_1 + \Gamma_2\mathbf{N}_2$ can be expanded in a Taylor series form (in powers of ϵ^2):

$$\Theta(\lambda) = \Theta^{(0)} + \Theta^{(1)}\epsilon^2 + \Theta^{(2)}\epsilon^4 + \cdots + O(\epsilon^{2n}), \tag{15}$$

where $\Theta^{(m)} = [R_m, S_m]^T e^{\mathrm{i}(\theta_0 z + \phi_0 t)}$ denotes the series coefficient of order m. As a result, the nth-order rogue wave solution can be expressed as

$$E^{[n]} = E_0\left(-1 - \frac{i}{|E_0|}\mathbf{Y}_1(\mathbf{M}^\dagger)^{-1}\mathbf{Y}_2^\dagger\right)\left(-\frac{\det(\mathbf{M}^\dagger)}{\det(\mathbf{M})}\right)^{\mu/\gamma}, \tag{16}$$

where the dagger sign † indicates the complex-conjugate transpose, 'det' means taking the determinant of a square matrix, $\mathbf{Y}_j$ ($j = 1, 2$) are $1 \times n$ row vectors defined through

$$\begin{bmatrix} \mathbf{Y}_1 \\ \mathbf{Y}_2 \end{bmatrix} = \left[\Theta^{(0)}, \Theta^{(1)}, \Theta^{(2)}, \cdots, \Theta^{(n-1)}\right], \tag{17}$$

and $\mathbf{M}$ is an $n \times n$ matrix with its entries M_{ij} determined by

$$\frac{\Theta^\dagger\mathbf{X}\Theta}{\lambda - \lambda^*} = \sum_{ij}^{n} M_{ij}\epsilon^{*2(i-1)}\epsilon^{2(j-1)} + O(|\epsilon|^{4n}), \quad \mathbf{X} = \gamma\begin{bmatrix} \sqrt{\lambda} & 0 \\ 0 & \sqrt{\lambda^*} \end{bmatrix}. \tag{18}$$

We would like to emphasize that the compact expression (16) for the nth-order rogue wave solution was never reported before, to our best knowledge, which is seen to be distinctly different from the previous solution forms obtained for the NLS equations or their extensions [40, 59].

3. Super chirped rogue wave dynamics

As an illustrative example of our general solution (16), we demonstrate in Fig. 1 the first-order (fundamental), second-order, and third-order rogue wave dynamics, respectively, obtained with the same set of system parameters $a = 1$, $\sigma = 1$, $\gamma = 1$, $\mu = 3/2$, and $\omega = -1$, but with different structural parameters γ_j. For convenience, the explicit solution forms for these three low-order rogue waves have been provided in Appendix A (see Eqs. (A3)–(A5)). It is seen that, for given structural parameters as specified in the caption, the fundamental rogue wave always takes the shape of Peregrine soliton (see Fig. 1(a)), while the second-order and third-order rogue waves appear as the rogue wave triplet (see Fig. 1(b)) and sextet (see Fig. 1(c)), which consist of 3 and 6 Peregrine solitons, respectively. Depending on the relative values of the structural parameters γ_j, the multiple rogue wave dynamics can display patterns that might not be so regular as seen in Figs. 1(b) and 1(c). Generally, for an nth-order rogue wave, it can evolve into at most $n(n + 1)/2$ Peregrine solitons, each with a peak amplitude three times the level of the background field [36].

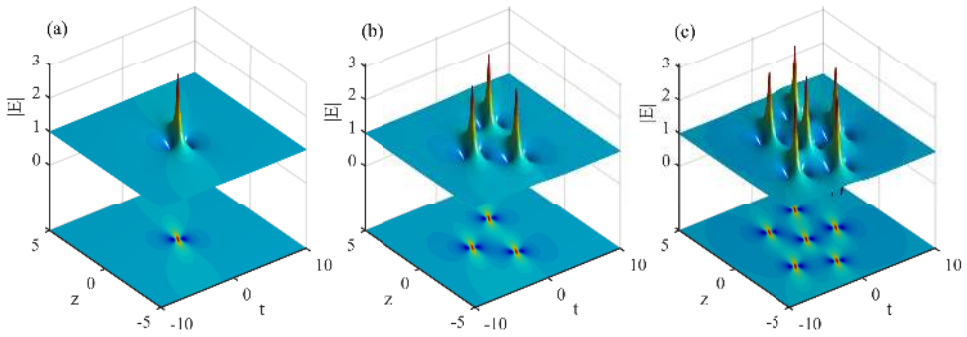

Fig. 1. Surface (top) and contour (bottom) plots of the (a) first-order (fundamental), (b) second-order, and (c) third-order rogue waves in the self-focusing (or anomalous dispersion) regime, obtained with the same set of system parameters. (a) $\gamma_2 = 1$; (b) $\gamma_2 = 1$, $\gamma_3 = 100$; (c) $\gamma_2 = 1$, $\gamma_5 = 2000$. In each case, the other unshown γ_j will be set zero.

More interestingly, we find further that, by a specific choice of parameters γ_j, the nth-order rogue wave can reach a climax of $2n + 1$ times the background height. In contrast to the above-mentioned multiple rogue wave dynamics, this kind of rogue wave state manifests itself as a single main hump, and hence can be referred to as a *super rogue wave* [37] when $n > 1$. Physically, such super rogue wave state results from the superposition of $n(n + 1)/2$ Peregrine solitons. Figure 2 shows the preceding three low-order rogue wave states on the same plane-wave background formed in the normal dispersion regime ($\sigma = -1$), which have peak amplitudes higher by a factor of 3, 5, and 7, respectively, as compared to the background height. In these plots, we have used special sets of structural parameters given in the caption that can give rise to the unique super rogue wave states as shown, after translations on the plane (z, t). As one can check via Eqs. (A3)–(A5) in Appendix A, these rogue wave states can not have a peak amplitude higher than their respective factors specified above, no matter what values of γ_j are used and no matter whether the nonlinear system is self-focusing or not. In addition, different from the symmetric super rogue waves in the NLS system [37, 39], the super rogue waves associated to Eq. (1) are generally anti-symmetrical in shape, as indicated in Figs. 2(b) and 2(c).

Optics EXPRESS

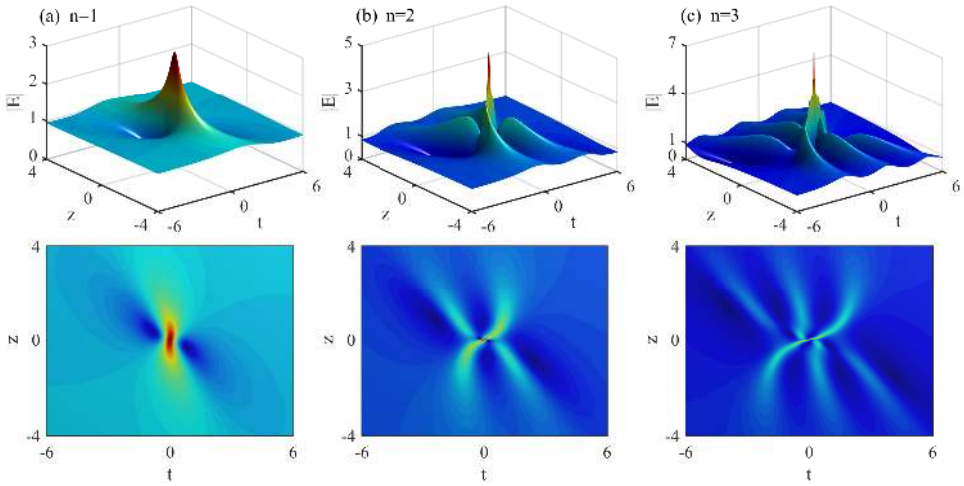

Fig. 2. The preceding three low-order rogue wave states that have their respective maximum allowable amplitude factor (3, 5, 7) in the normal dispersion regime: (a) Peregrine soliton; (b) Super second-order rogue wave; (c) Super third-order rogue wave. We choose $a = 1$, $\sigma = -1$, $\gamma = 1$, $\mu = 3/2$ and $\omega = -2$ as the system parameters, and choose $\gamma_2 = 1$, $\gamma_3 = 2/81 - i86\sqrt{2}/81$, $\gamma_5 = 359/1215 - i101\sqrt{2}/1215$, and $\gamma_1 = \gamma_4 = \gamma_6 = 0$ as the specific structural parameters.

Moreover, aside from the anti-symmetrical amplitude (or intensity) distribution, these super rogue waves are generally endowed with an extra nonlinear phase as well, as implied by the exponential factor $[-\det(\mathbf{M}^\dagger)/\det(\mathbf{M})]^{\mu/\gamma}$ in solution (16). More exactly, as will be shown below, this extra phase is actually caused by the exponential factor $[-\det(\mathbf{M}^\dagger)/\det(\mathbf{M})]^{\mu/\gamma-1}$, i.e., equal to the phase of $\det(\chi\mathbf{M}^\dagger)$ multiplied by $2(\mu/\gamma - 1)$. It is time and space dependent, and hence would lead the rogue waves to undergo a frequency shift (or chirping) during evolution. Such a chirping effect does not exist in many integrable systems, e.g., in the NLS equation [37], in the Maxwell–Bloch system [25], and in the Manakov system [59,62]. For this reason, our super rogue wave solutions discussed here can be termed *super chirped rogue waves*, to show distinction. In the following, let us take a closer look at this super chirped rogue wave dynamics.

First of all, we find that the super rogue waves (including the fundamental solution) actually have a unique solution form, which does not involve any structural parameters γ_j. For instance, by performing the replacements $z \to z - z_0$ and $t \to t - t_0$, where z_0 and t_0 are the magnitudes of translation along the z and t axes, respectively, given by

$$z_0 = \frac{a^2\gamma}{2\beta(a^4\gamma^2+\beta^2)} - \frac{\mathrm{Im}(\gamma_1/\gamma_2)}{2\beta^2}, \quad t_0 = z_0(a^2\mu+\omega) - \frac{\beta}{2(a^4\gamma^2+\beta^2)} - \frac{\mathrm{Re}(\gamma_1/\gamma_2)}{2\beta}, \tag{19}$$

the fundamental rational solution given by Eq. (A3) in Appendix A can be simplified as

$$E^{[1]} = E_0\left[1 - \frac{2i(\gamma\tau + \beta^2 z/a^2) + 1/a^2}{M - iN}\right]\exp(i\Phi), \tag{20}$$

where

$$\begin{aligned} &\tau = t - (a^2\mu+\omega)z, \qquad M = \left(\frac{\beta^2}{a^2} + \gamma^2 a^2\right)(\tau^2 + \beta^2 z^2) + \frac{1}{4a^2}, \\ &N = \gamma(\gamma a^2 z - \tau), \qquad \Phi = 2\left(\frac{\mu}{\gamma} - 1\right)\arctan\left(\frac{N}{M}\right). \end{aligned} \tag{21}$$

Here Im and Re denote the imaginary and real parts of a complex number, respectively. It is clear that this simplified fundamental solution has now become independent of any structural parameter, displaying a 3-fold peak amplitude that has been located on the origin and an extra phase Φ that is proportional to the factor $2(\mu/\gamma - 1)$. Indeed, as one can see, this rational solution is none other than the chirped Peregrine soliton solution obtained in [29] via a gauge transformation method. Noteworthily, as discussed in [29], the solution (20) has also an inherent phase caused by the complex term inside square brackets, but that phase is intrinsic to all Peregrine soliton categories and thus will not be used to define what we mean by chirped Peregrine soliton.

On the basis of the above translations defined by Eq. (19), if one further sets $\gamma_2 = 1$ without loss of generality, and then expresses γ_3 by

$$\gamma_3 = \frac{3\gamma_1}{2} + \gamma_1\gamma_4 - \frac{\gamma_1^3}{3} - \gamma_1^* - \frac{2\beta^2(3a^8\gamma^4 - 6a^4\beta^2\gamma^2 - \beta^4)}{3(a^4\gamma^2 + \beta^2)^3} - \frac{2ia^2\beta\gamma(3a^8\gamma^4 + 14a^4\beta^2\gamma^2 + 3\beta^4)}{3(a^4\gamma^2 + \beta^2)^3},$$

the second-order rogue wave solution given by Eq. (A4) can reduce to the super rogue wave state:

$$E^{[2]} = E_0\left(1 - \frac{G + iH}{C - iD}\right)\exp(i\Phi), \tag{22}$$

which involves an extra nonlinear phase that is again proportional to $2(\mu/\gamma - 1)$:

$$\Phi = 2\left(\frac{\mu}{\gamma} - 1\right)\arctan\left(\frac{D}{C}\right). \tag{23}$$

Here C, D, G, and H are real polynomials of z and $\tau \equiv t - (a^2\mu + \omega)z$, given by

$$\begin{aligned}
C =\ & 64(a^4\gamma^2 + \beta^2)^3(\beta^2z^2 + \tau^2)^3 + (a^4\gamma^2 + \beta^2)\left[48\beta^2(4a^8\gamma^4 + 17a^4\beta^2\gamma^2 + 9\beta^4)z^4\right.\\
&\left.+384a^6\beta^2\gamma^3\tau z^3 - 288(2a^4\gamma^2 + \beta^2)(a^4\gamma^2 + \beta^2)\tau^2z^2 + 384a^6\gamma^3\tau^3z - 48(3a^4\gamma^2 - \beta^2)\tau^4\right]\\
&+ 36(28a^8\gamma^4 + 35a^4\beta^2\gamma^2 + 11\beta^4)z^2 - 288a^6\gamma^3\tau z + 36(7a^4\gamma^2 + 3\beta^2)\tau^2 + 9,\\
D =\ & 192a^2\gamma(a^4\gamma^2 + \beta^2)^2(\beta^2z^2 + \tau^2)^2(a^2\gamma z - \tau) + 96a^2\gamma\left[a^2\gamma(6a^8\gamma^4 + 13a^4\beta^2\gamma^2 + 9\beta^4)z^3\right.\\
&\left.+(6a^8\gamma^4 + 15a^4\beta^2\gamma^2 + 3\beta^4)\tau z^2 + 3a^2\gamma(a^4\gamma^2 - \beta^2)\tau^2z - (3a^4\gamma^2 + \beta^2)\tau^3\right]\\
&+ 36a^2\gamma(11a^2\gamma z - 3\tau),\\
G =\ & 192(a^4\gamma^2 + \beta^2)^2(\beta^2z^2 + \tau^2)(4a^2\gamma\tau z + 5\beta^2z^2 + \tau^2) - 1152a^4\beta^2\gamma^2z^2\\
&+ 288(3a^4\gamma^2 + \beta^2)\left[(2a^4\gamma^2 + 3\beta^2)z^2 - 2a^2\gamma\tau z + \tau^2\right] - 36,\\
H =\ & 384(a^4\gamma^2 + \beta^2)^2(\beta^2z^2 + \tau^2)^2(a^2\gamma\tau + \beta^2z) + 192\left[(4a^8\gamma^4 + 3a^4\beta^2\gamma^2 + \beta^4)\beta^2z^3\right.\\
&\left.-3a^2\gamma(a^4\gamma^2 + 3\beta^2)(2a^4\gamma^2 + \beta^2)\tau z^2 - 3(2a^8\gamma^4 + a^4\beta^2\gamma^2 + \beta^4)\tau^2z + a^2\gamma(a^4\gamma^2 - \beta^2)\tau^3\right]\\
&- 72\left[(12a^4\gamma^2 + 5\beta^2)z + a^2\gamma\tau\right].
\end{aligned} \tag{24}$$

Obviously, the simplified rational solution (22) does not involve any structural parameters γ_j. As the polynomial C is always positive definite for arbitrary system parameters, this solution can now describe the super second-order rogue wave dynamics in either the anomalous or normal dispersion regime. It is easy to check that this super rogue wave will have a 5-fold peak amplitude, as shown in Fig. 2(b). In addition, it will undergo a frequency chirp defined by [44]

$$\delta\omega = -\frac{\partial\Phi}{\partial t} = \frac{2(\mu - \gamma)(DC_t - CD_t)}{\gamma(C^2 + D^2)}, \tag{25}$$

which is also localized in both time and space. This chirp is different from that of traveling solitons, which is usually of tanh shape in the transversal dimension, namely, nearly linear across

the pulse width [30, 31]. Here, for the same reason that applies to the chirped Peregrine soliton, we do not consider the intrinsic chirping effect arising from the complex term inside the big round brackets in Eq. (22). Figure 3 shows the super second-order rogue wave solutions in the self-focusing (or anomalous dispersion) regime for the GI equation ($\mu = 0$), the CLL-NLS equation ($\mu = \gamma$), and the KN-NLS equation ($\mu = 2\gamma$), respectively, with the other system parameters kept the same, i.e., $a = 1$, $\sigma = 1$, $\gamma = 1$, and $\omega = -1$. It is exhibited that all these super rogue waves have a 5-fold peak amplitude, in addition to an extended spatiotemporal distribution as μ increases. Meanwhile, depending on the GI, CLL, and KN models used, the chirp of these rogue waves will exhibit a dark doubly localized structure, zero, and a bright doubly localized structure correspondingly, as suggested by surface plots in the right column of Fig. 3.

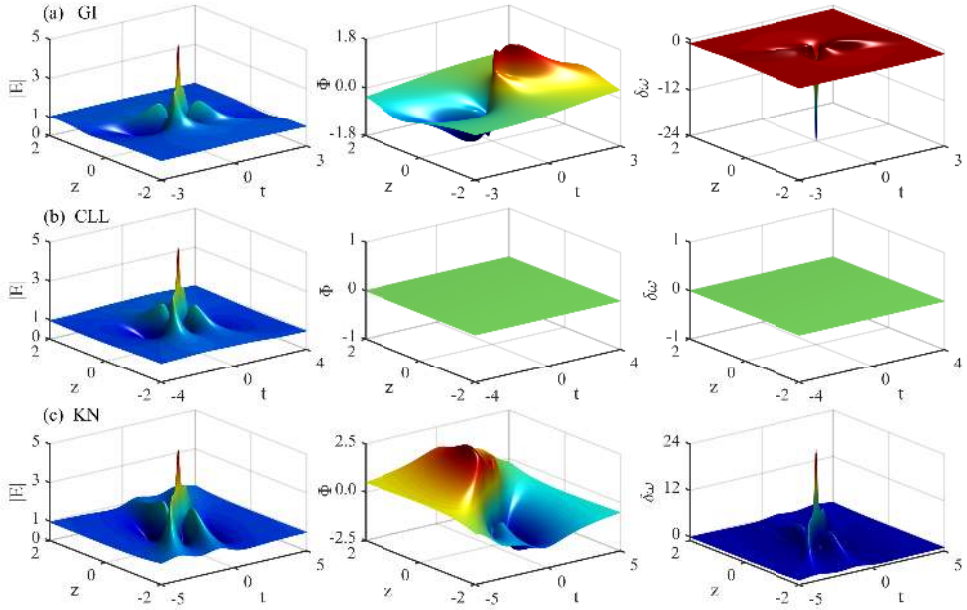

Fig. 3. Super second-order rogue waves in the anomalous dispersion regime associated to (a) the GI equation, (b) the CLL-NLS equation, and (c) the KN-NLS equation, respectively. Left column: Amplitude $|E|$; Middle column: Phase Φ; Right column: Chirp $\delta\omega$.

As a limiting case, when $\gamma = 0$ (which corresponds to the KE equation scenario), it follows that $D = 0$ and $\beta = a\sqrt{\sigma}$. Then, the second-order rogue wave solution (22) can boil down to

$$E^{[2]} = E_0\left(1 - \frac{G + iH}{C}\right)\exp(i\Phi), \tag{26}$$

where

$$\begin{aligned} C &= 64\beta^6(\beta^2z^2 + \tau^2)^3 + 48\beta^4(3\beta^2z^2 - \tau^2)^2 + 36\beta^2(11\beta^2z^2 + 3\tau^2) + 9,\\ G &= 192\beta^4(\beta^2z^2 + \tau^2)(5\beta^2z^2 + \tau^2) + 288\beta^2(3\beta^2z^2 + \tau^2) - 36,\\ H &= 384\beta^6(\beta^2z^2 + \tau^2)^2z + 24\beta^2z(8\beta^4z^2 - 24\beta^2\tau^2 - 15),\\ \Phi &= -\frac{\mu a^2}{\beta^2}(\ln C)_t = -\frac{24\mu a^2\tau}{C}[16\beta^4(\beta^2z^2 + \tau^2)^2 - 8\beta^2(3\beta^2z^2 - \tau^2) + 9]. \end{aligned} \tag{27}$$

It is clear that the polynomial C will be positive definite when $\sigma > 0$, but fails to be so if $\sigma < 0$. Therefore, only in the self-focusing (or anomalous dispersion) regime does the rational solution

(26) represent a genuine rogue wave, as occurred in the NLS situation [3]. Besides, the extra nonlinear phase Φ would lead to a frequency chirp given by

$$\delta\omega = \frac{\mu a^2}{\beta^2}(\ln C)_{tt}. \tag{28}$$

As seen in Fig. 4, this special super second-order rogue wave is symmetric in amplitude distribution (see left column), as in the NLS equation, but, however, has a nonvanishing nonlinear phase (see middle column) and thus a doubly localized chirp (see right column) that will be absent in the NLS equation. Naturally, if we further let $\mu = 0$, the solution (26) can be reduced to that of the NLS equation, in which the nonlinear phase Φ is vanishing.

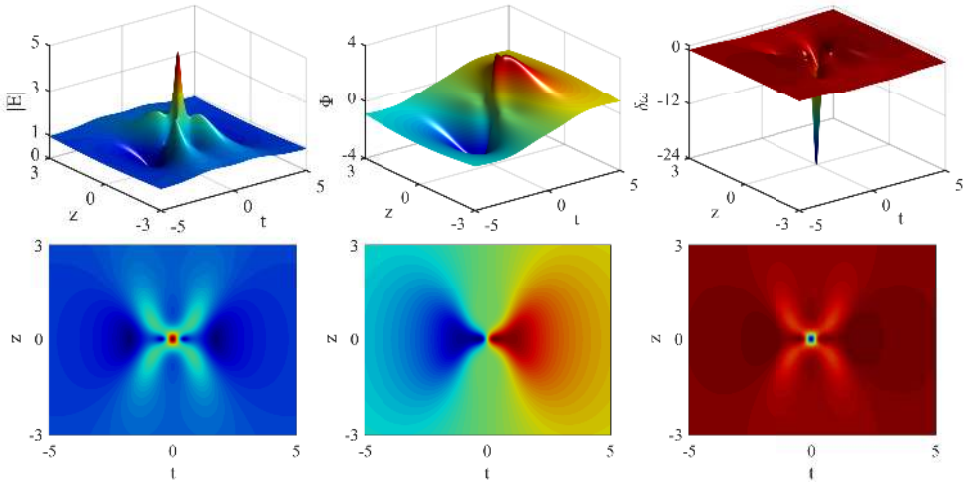

Fig. 4. Super second-order rogue wave solution of the KE equation in the anomalous dispersion regime, with the system parameters $a = 1$, $\sigma = 1$, $\gamma = 0$, $\mu = -1$ and $\omega = 1$.

In a similar fashion, one can readily obtain the super third-order rogue wave solution from Eq. (16) or from Eq. (A5) in Appendix A, which will also be unique in form, although lengthy. It is easy to show that this simplified super rogue wave solution will involve a 7-fold peak amplitude, as shown in Fig. 2(c), and, if $\mu \neq \gamma$, a nonlinear phase Φ that may result in a chirp. Here, for the sake of brevity, we do not present this simplified yet lengthy solution.

4. Numerical simulations

We performed extensive numerical simulations to inspect the stability of super chirped rogue waves against white-noise perturbations, based on the split-step Fourier method [11]. Here, in contrast to the intuitionistic "stability" concept intended for usual solitons, we would refer to the rogue wave as being *stable* if its structure can unfold without significant distortion over a rather long distance, irrespective of whether this type of wave-packet is transient or not.

As typical examples, we chose to simulate the GI and KE super chirped rogue waves whose structures are already shown in Figs. 3(a) and 4, respectively. We put the noise onto the initial profile by multiplying the real and imaginary parts of the optical field E by a factor $[1 + \varepsilon r_i(x)]$ $(i = 1, 2)$, respectively, where $r_{1,2}$ are two uncorrelated random functions uniformly distributed in the interval $[-1,\ 1]$ and ε is a small parameter defining the noise level. Figure 5 displays the numerical results, where, in order to show up other periodical wave structures arising from MI, we used a quite large noise level in both situations, namely, $\varepsilon = 0.01$ for the GI super

chirped rogue wave and $\varepsilon = 0.02$ for the KE super chirped rogue wave. The initial amplitude profiles used for our simulations are indicated by red lines in Figs. 5(a) and 5(d), each having been compared to their respective analytical solutions given at $z = -2$ and -5 (see blue lines). It is exhibited that, even under such a large noise perturbation, these super chirped rogue waves can still propagate very neatly for a rather long distance, despite the onset of the spontaneous MI activated by the white noise, as seen in Figs. 5(b) and 5(e). To evaluate the consistency, we plotted in Figs. 5(c) and 5(f) the numerical amplitude profiles obtained at $t = 0$ (red lines), which agree very well with the analytical solutions (blue lines). Besides, we notice that, compared with its GI cousin, the KE super chirped rogue wave can recover from larger noise level on a less unstable background and thus can propagate over longer distance without significant distortion. For example, for the case shown in Fig. 5(e), such a distortion-free propagation can unfold within around 8 dispersion lengths, or more intuitively, around 0.4 km for a 1.55 μm pulse of duration 1 ps propagating in a telecommunication fiber with GVD of -20 ps^2/km.

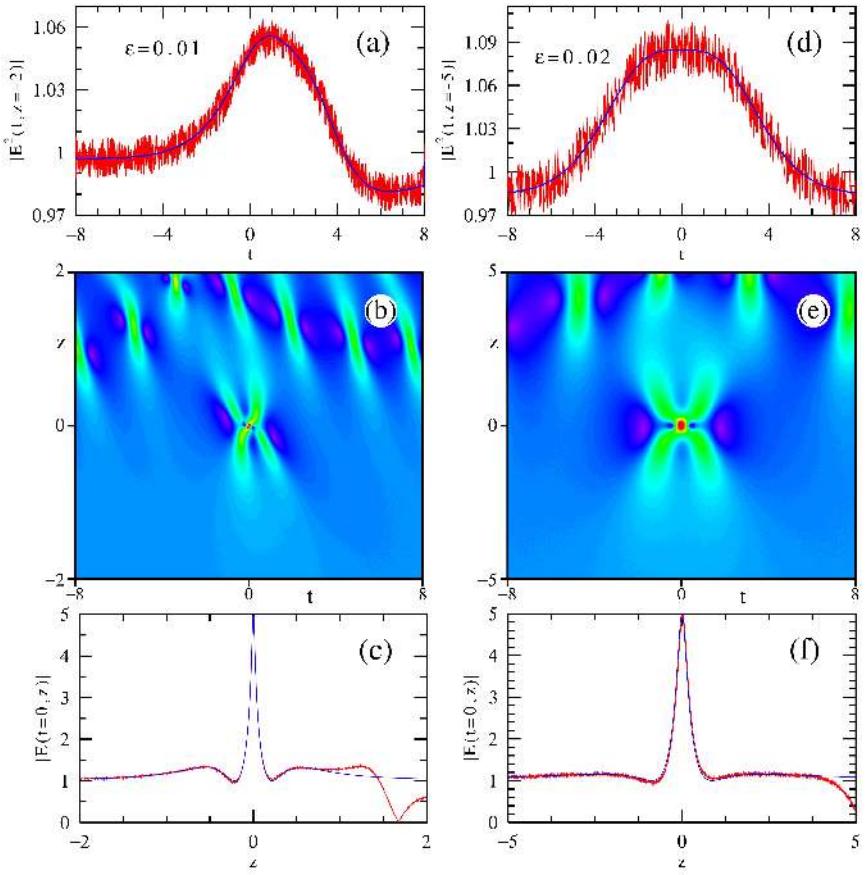

Fig. 5. Numerical simulations of the GI (see left column) and KE (see right column) super chirped second-order rogue waves, which are the same as in Figs. 3(a) and 4, but are now perturbed by white noises of $\varepsilon = 0.01$ and 0.02, respectively. (a), (d): Initial amplitude profiles (red line) as compared to the analytical ones (blue line); (b), (e): Numerical recurrence of rogue waves from the above initial conditions; (c), (f): the numerical amplitude profiles obtained at $t = 0$ (red line) compared with their analytical ones (blue line).

Further, we have also investigated the robustness of these super chirped rogue waves by

inspecting if they can appear spontaneously in a turbulent field. For this purpose, we have performed a number of simulations, integrating Eq. (1) numerically with an initial field that can be defined by the plane-wave solution (4) perturbed by a white noise of very low amplitude. This low-amplitude noise may produce a turbulent field via an MI process and then one can monitor the maximums of the field amplitude for all t at each z value (i.e., $|E(z)|_{\text{peak}}$) so as to detect the presence of extreme waves in such a field. Here we still take the GI super chirped rogue wave shown in Fig. 3(a) as an example and use the same noise level $\varepsilon = 0.01$ as in Fig. 5(a). For some realizations, we got typically what is shown in Fig. 6(a). It is seen that the continuous wave remains stationary for a short propagation distance, and then it develops exponentially to create a turbulent field, as expected. Quite strikingly, in this turbulent field, one can clearly observe extreme peaks with amplitudes close to 5, which can be associated to super rogue waves. One of them can be seen at around $z = 14$ (see the yellow region). We presented the evolution of the field amplitude around this z value and in a narrow temporal interval properly chosen in Fig. 6(b), where the rogue wave encircled by the black curve bears a strong resemblance to the GI super chirped rogue wave shown in Fig. 5(b) or in Fig. 3(a), despite there being random fields surrounding it. Accordingly, as one might envision, this impressive robustness of super chirped rogue waves may enable them to be observed in realistic physical settings (e.g., in optical fibers), as long as the self-steepening effect functions properly.

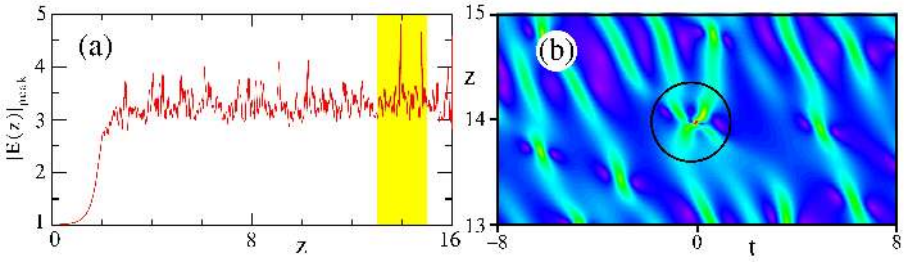

Fig. 6. Numerical excitation of the GI super chirped rogue wave from a turbulent field under otherwise the same parameter condition as in Fig. 3(a). The panel (a) shows the maximum peak amplitude chosen from a very large t window for each specific value of z, and (b) displays the evolution of the field amplitude around $z = 14$ within a narrow temporal interval, where a typical super chirped rogue wave has been singled out by the black curve.

5. Conclusion

We have studied the super rogue wave dynamics of optical pulses in optical fibers within the framework of a generalized CQ NLS equation that contains the GVD, the Kerr and quintic nonlinearity, and the self-steepening effect. With the help of the nonrecursive Darboux transformation technique, we have presented for the first time the nth-order rogue wave solution and particularly its explicit solution forms up to the third order. It is unveiled that, for a rogue wave solution of order n, it can be shaped up as a single super rogue wave state whose peak amplitude is as high as $2n + 1$ times the background level, which results from the superposition of $n(n + 1)/2$ Peregrine solitons. More interestingly, we have found that these super rogue waves involve a frequency chirp that is also localized in both time and space.

In addition, we have performed numerical simulations to confirm the stability of these super chirped rogue waves in spite of the onset of the spontaneous MI activated by white noises, and have demonstrated their numerical excitation from a turbulent field caused by a low-amplitude noise. In the light of this impressive recurrence stability and the universality of the model used, we anticipate that these super chirped rogue waves can be observed in optical fibers, e.g., in

highly nonlinear chalcogenide fibers [44], where the cubic-quintic nonlinearity (including the self-steepening effect) is important, while the higher-order dispersions beyond GVD can be ignored, for pulses in the picosecond range and for small propagation distances. We would also like to remark that such super chirped rogue waves could be observed as well in quadratic crystals (e.g., β-barium borate or periodically poled lithium tantalate crystals) in the high phase-mismatch cascading regime, which may produce a controllable self-steepening effect [45–47].

On the other side, as Eq. (1) has significantly generalized such integrable models as the NLS equation, the CLL–NLS equation, the KN–NLS equation, the GI equation, and the KE equation, we expect that the universal solutions presented here might be used as a platform for exploring the interesting rogue wave dynamics of many complex and non-integrable systems, which, to the first order approximation, are well described by the latter equations [64, 65].

Appendix A—Explicit rogue wave solutions up to the third order

In this Appendix, we would like to derive the explicit rogue wave solutions up to the third order from Eq. (16). As seen, only the preceding three series coefficients $\Theta^{(0,1,2)} \equiv [R_{0,1,2}, S_{0,1,2}]^T e^{\mathrm{i}(\theta_0 z+\phi_0 t)}$ in Eq. (15) need to be determined, which, after some algebra, can be found as below:

$$\begin{aligned}
R_0 &= \gamma_1 + 2i\gamma_2\beta\vartheta,\\
S_0 &= -\gamma_1 - 2i\gamma_2\beta\xi,\\
R_1 &= -2\gamma_1\beta^2\vartheta^2 + \gamma_2\left(-\frac{4i}{3}\beta^3\vartheta^3 + 5i\beta\vartheta + 4\beta\tau\right) + \gamma_3 + 2i\gamma_4\beta\vartheta,\\
S_1 &= 2\gamma_1\beta^2\xi^2 - \gamma_2\left(-\frac{4i}{3}\beta^3\xi^3 + 5i\beta\xi + 4\beta\tau - i\rho\right) - \gamma_3 - 2i\gamma_4\beta\xi,\\
R_2 &= \gamma_1 g + \gamma_2 p - 2\gamma_3\beta^2\vartheta^2 + \gamma_4\left(-\frac{4i}{3}\beta^3\vartheta^3 + 5i\beta\vartheta + 4\beta\tau\right) + \gamma_5 + 2i\gamma_6\beta\vartheta,\\
S_2 &= -\gamma_1 h - \gamma_2 q + 2\gamma_3\beta^2\xi^2 - \gamma_4\left(-\frac{4i}{3}\beta^3\xi^3 + 5i\beta\xi + 4\beta\tau - i\rho\right) - \gamma_5 - 2i\gamma_6\beta\xi,
\end{aligned} \tag{A1}$$

where γ_j $(j = 1, 2, \cdots, 6)$ are arbitrary complex constants, and

$$\begin{aligned}
&\kappa = -\gamma a^2 + i\beta, \qquad \rho = \frac{4\beta}{\kappa} + \frac{4i\beta^2}{\kappa^2} + \frac{8\beta^3}{3\kappa^3},\\
&\tau = t - (a^2\mu + \omega)z, \qquad \vartheta = i\tau - \beta z, \qquad \xi = \vartheta + 1/\kappa,\\
&g = \frac{2\beta^4\vartheta^4}{3} - 10\beta^2\vartheta^2 + 8i\beta^2\vartheta\tau,\\
&h = \frac{2\beta^4\xi^4}{3} - 10\beta^2\xi^2 + 8i\beta^2\xi\tau + 2\rho\beta\xi,\\
&p = \frac{4i\beta^5\vartheta^5}{15} - 10i\beta^3\vartheta^3 + \frac{7i\beta\vartheta}{4} - 8\beta^3\vartheta^2\tau + 2\beta\tau,\\
&q = \frac{4i\beta^5\xi^5}{15} - 10i\beta^3\xi^3 + \frac{7i\beta\xi}{4} - 8\beta^3\xi^2\tau + 2\beta\tau + 2i\rho\beta^2\xi^2\\
&\quad - \frac{2i\beta}{\kappa} + \frac{2\beta^2}{\kappa^2} - \frac{12i\beta^3}{\kappa^3} - \frac{16\beta^4}{\kappa^4} + \frac{32i\beta^5}{5\kappa^5}.
\end{aligned} \tag{A2}$$

Accordingly, the expressions of $\mathbf{Y}_{1,2}$ and $\mathbf{M}$ intended for the former three low-order rogue wave solutions can be found as well, via Eqs. (17) and (18). Therefore, from Eq. (16), one can obtain the explicit fundamental rogue wave solution of Eq. (1) as

$$E^{[1]} = E_0\left(-1 + \frac{i\chi R_0 S_0^*}{\gamma a m_{11}^*}\right)\left(\frac{m_{11}^*}{m_{11}}\right)^{\mu/\gamma}, \tag{A3}$$

the explicit second-order rogue wave solution as

$$E^{[2]} = E_0\left\{-1+\frac{i\chi[R_0(S_0^*m_{22}^*-S_1^*m_{21}^*)+R_1(S_1^*m_{11}^*-S_0^*m_{12}^*)]}{\gamma a(m_{11}^*m_{22}^*-m_{12}^*m_{21}^*)}\right\}\left(-\frac{m_{11}^*m_{22}^*-m_{12}^*m_{21}^*}{m_{11}m_{22}-m_{12}m_{21}}\right)^{\mu/\gamma}, \tag{A4}$$

and the explicit third-order rogue wave solution as

$$\begin{aligned} E^{[3]} = E_0&\left(-1+\frac{i\chi}{\gamma a}\begin{bmatrix} R_0, R_1, R_2 \end{bmatrix}\begin{bmatrix} m_{11}^*, m_{21}^*, m_{31}^* \\ m_{12}^*, m_{22}^*, m_{32}^* \\ m_{13}^*, m_{23}^*, m_{33}^* \end{bmatrix}^{-1}\begin{bmatrix} S_0^* \\ S_1^* \\ S_2^* \end{bmatrix}\right) \\ &\times\left(\begin{vmatrix} m_{11}, m_{12}, m_{13} \\ m_{21}, m_{22}, m_{23} \\ m_{31}, m_{32}, m_{33} \end{vmatrix}^* \Big/ \begin{vmatrix} m_{11}, m_{12}, m_{13} \\ m_{21}, m_{22}, m_{23} \\ m_{31}, m_{32}, m_{33} \end{vmatrix}\right)^{\mu/\gamma}, \end{aligned} \tag{A5}$$

where $||[m_{ij}]||$ signifies the determinant of the involved matrix and m_{ij} are defined by

$$\begin{aligned} m_{11} &= \sqrt{\lambda_0}|R_0|^2+\sqrt{\lambda_0^*}|S_0|^2, \\ m_{12} &= \sqrt{\lambda_0}R_0^*R_1+\sqrt{\lambda_0^*}S_0^*S_1+\frac{\chi|R_0|^2}{2\sqrt{\lambda_0}}-m_{11}, \\ m_{13} &= \sqrt{\lambda_0}R_0^*R_2+\sqrt{\lambda_0^*}S_0^*S_2+\frac{\chi R_0^*}{2\sqrt{\lambda_0}}\left(R_1-\frac{\chi R_0}{4\lambda_0}\right)-m_{12}, \\ m_{21} &= \sqrt{\lambda_0}R_0R_1^*+\sqrt{\lambda_0^*}S_0S_1^*-\frac{\chi|S_0|^2}{2\sqrt{\lambda_0^*}}-m_{11}, \\ m_{22} &= \sqrt{\lambda_0}|R_1|^2+\sqrt{\lambda_0^*}|S_1|^2+\frac{\chi}{2}\left(\frac{R_0R_1^*}{\sqrt{\lambda_0}}-\frac{S_0^*S_1}{\sqrt{\lambda_0^*}}\right)-m_{12}-m_{21}, \\ m_{23} &= \sqrt{\lambda_0}R_1^*R_2+\sqrt{\lambda_0^*}S_1^*S_2-\frac{\chi S_0^*S_2}{2\sqrt{\lambda_0^*}}+\frac{\chi R_1^*}{2\sqrt{\lambda_0}}\left(R_1-\frac{\chi R_0}{4\lambda_0}\right)-m_{22}-m_{13}, \\ m_{31} &= \sqrt{\lambda_0}R_0R_2^*+\sqrt{\lambda_0^*}S_0S_2^*-\frac{\chi S_0}{2\sqrt{\lambda_0^*}}\left(S_1^*+\frac{\chi S_0^*}{4\lambda_0^*}\right)-m_{21}, \\ m_{32} &= \sqrt{\lambda_0}R_1R_2^*+\sqrt{\lambda_0^*}S_1S_2^*+\frac{\chi R_0R_2^*}{2\sqrt{\lambda_0}}-\frac{\chi S_1}{2\sqrt{\lambda_0^*}}\left(S_1^*+\frac{\chi S_0^*}{4\lambda_0^*}\right)-m_{22}-m_{31}, \\ m_{33} &= \sqrt{\lambda_0}|R_2|^2+\sqrt{\lambda_0^*}|S_2|^2+\frac{\chi R_2^*}{2\sqrt{\lambda_0}}\left(R_1-\frac{\chi R_0}{4\lambda_0}\right)-\frac{\chi S_2}{2\sqrt{\lambda_0^*}}\left(S_1^*+\frac{\chi S_0^*}{4\lambda_0^*}\right)-m_{23}-m_{32}. \end{aligned} \tag{A6}$$

It should be noted that in the above formulas for m_{ij}, one can use $\sqrt{\lambda_0}=\beta/a+i\gamma a$ and $\sqrt{\lambda_0^*}=\beta/a-i\gamma a$, which have been separated into real and imaginary parts. As one might check, the solutions given by Eqs. (A3)–(A5) have no singularity problems.

Funding

National Natural Science Foundation of China (NSFC) (11474051); MINECO (TEC2015-71127-C2-1-R); Comunidad Autonoma de Madrid (CAM) (S2013/MIT-2790).

Optics EXPRESS

References

1. C. Kharif, E. Pelinovsky, and A. Slunyaev, *Rogue Waves in the Ocean* (Springer, 2009).
2. D. R. Solli, C. Ropers, P. Koonath, and B. Jalali, "Optical rogue waves," Nature (London) **450**, 1054–1057 (2007).
3. S. Chen, F. Baronio, J. M. Soto-Crespo, Ph. Grelu, and D. Mihalache, "Versatile rogue waves in scalar, vector, and multidimensional nonlinear systems," J. Phys. A Math. Theor. **50**, 463001 (2017).
4. J. M. Dudley, F. Dias, M. Erkintalo, and G. Genty, "Instabilities, breathers and rogue waves in optics," Nat. Photonics **8**, 755–764 (2014).
5. S. Wabnitz, ed., *Nonlinear Guided Wave Optics: A Testbed for Extreme Waves* (IOP Publishing, 2017).
6. Yu. S. Kivshar and G. P. Agrawal, *Optical Solitons: From Fibers to Photonic Crystals* (Academic, 2003).
7. B. A. Malomed, D. Mihalache, F. Wise, and L. Torner, "Spatiotemporal optical solitons," J. Opt. Soc. Am. B **7**, R53–R72 (2005).
8. Z. Chen, M. Segev, and D. N. Christodoulides, "Optical spatial solitons: historical overview and recent advances," Rep. Prog. Phys. **75**, 086401 (2012).
9. B. A. Malomed, "Multidimensional solitons: Well-established results and novel findings," Eur. Phys. J. Spec. Top. **225**, 2507–2532 (2016).
10. D. Mihalache, "Multidimensional localized structures in optical and matter-wave media: A topical survey of recent literature," Rom. Rep. Phys. **69**, 403 (2017).
11. J. M. Soto-Crespo, N. Devine, and N. Akhmediev, "Integrable turbulence and rogue waves: breathers or solitons?" Phys. Rev. Lett. **116**, 103901 (2016).
12. N. Akhmediev, A. Ankiewicz, and M. Taki, "Waves that appear from nowhere and disappear without a trace," Phys. Lett. A **373**, 675–678 (2009).
13. B. Kibler, J. Fatome, C. Finot, G. Millot, F. Dias, G. Genty, N. Akhmediev, and J. M. Dudley, "The Peregrine soliton in nonlinear fibre optics," Nat. Phys. **6**, 790–795 (2010).
14. C. Lecaplain, Ph. Grelu, J. M. Soto-Crespo, and N. Akhmediev, "Dissipative rogue waves generated by chaotic pulse bunching in a mode-locked laser," Phys. Rev. Lett. **108**, 233901 (2012).
15. C. Bao, J. A. Jaramillo-Villegas, Y. Xuan, D. E. Leaird, M. Qi, and A. M.Weiner, "Observation of Fermi-Pasta-Ulam recurrence induced by breather solitons in an optical microresonator," Phys. Rev. Lett. **117**, 163901 (2016).
16. D. Pierangeli, F. Di Mei, C. Conti, A. J. Agranat, and E. DelRe, "Spatial rogue waves in photorefractive ferroelectrics," Phys. Rev. Lett. **115**, 093901 (2015).
17. S. Birkholz, E. T. J. Nibbering, C. Brée, S. Skupin, A. Demircan, G. Genty, and G. Steinmeyer, "Spatiotemporal rogue events in optical multiple filamentation," Phys. Rev. Lett. **111**, 243903 (2013).
18. M. Leonetti and C. Conti, "Observation of three dimensional optical rogue waves through obstacles," Appl. Phys. Lett. **106**, 254103 (2015).
19. A. Safari, R. Fickler, M. J. Padgett, and R. W. Boyd, "Generation of caustics and rogue waves from nonlinear instability," Phys. Rev. Lett. **119**, 203901 (2017).
20. P. Suret, R. E. Koussaifi, A. Tikan, C. Evain, S. Randoux, C. Szwaj, and S. Bielawski, "Single-shot observation of optical rogue waves in integrable turbulence using time microscopy," Nat. Commun. **7**, 13136 (2016).
21. M. Onorato, S. Residori, U. Bortolozzo, A. Montina, and F. T. Arecchi, "Rogue waves and their generating mechanisms in different physical contexts," Phys. Rep. **528**, 47–89 (2013).
22. D. H. Peregrine, "Water waves, nonlinear Schödinger equations and their solutions," J. Aust. Math. Soc. B Appl. Math. **25**, 16–43 (1983).
23. V. I. Shrira and V. V. Geogjaev, "What makes the Peregrine soliton so special as a prototype of freak waves?" J. Eng. Math. **67**, 11–22 (2010).
24. A. Tikan, C. Billet, G. El, A. Tovbis, M. Bertola, T. Sylvestre, F. Gustave, S. Randoux, G. Genty, P. Suret, and J. M. Dudley, "Universality of the Peregrine soliton in the focusing dynamics of the cubic nonlinear Schrödinger equation," Phys. Rev. Lett. **119**, 033901 (2017).
25. S. Chen, Y. Ye, F. Baronio, Y. Liu, X.-M. Cai, and Ph. Grelu, "Optical Peregrine rogue waves of self-induced transparency in a resonant erbium-doped fiber," Opt. Express **25**(24), 29687–29698 (2017).
26. S. Chen, J. M. Soto-Crespo, F. Baronio, Ph. Grelu, and D. Mihalache, "Rogue-wave bullets in a composite (2+1)D nonlinear medium," Opt. Express **24**(14), 15251–15260 (2016).
27. B. Frisquet, B. Kibler, Ph. Morin, F. Baronio, M. Conforti, G. Millot, and S. Wabnitz, "Optical dark rogue wave," Sci. Rep. **6**, 20785 (2016).
28. S. Chen, Y. Ye, J. M. Soto-Crespo, Ph. Grelu, and F. Baronio, "Peregrine solitons beyond the threefold limit and their two-soliton interactions," Phys. Rev. Lett. **121**, 104101 (2018).
29. S. Chen, F. Baronio, J. M. Soto-Crespo, Y. Liu, and Ph. Grelu, "Chirped Peregrine solitons in a class of cubic-quintic nonlinear Schrödinger equations," Phys. Rev. E **93**, 062202 (2016).
30. Z. Li, L. Li, H. Tian, G. Zhou, and K. H. Spatschek, "Chirped femtosecond solitonlike laser pulse form with self-frequency shift," Phys. Rev. Lett. **89**, 263901 (2002).
31. S. Chen and L. Yi, "Chirped self-similar solutions of a generalized nonlinear Schrödinger equation model," Phys. Rev. E **71**, 016606 (2005).
32. J. D. Moores, "Nonlinear compression of chirped solitary waves with and without phase modulation," Opt. Lett. **21**(8), 555–557 (1996).
33. S. Chen and J. M. Dudley, "Spatiotemporal nonlinear optical self-similarity in three dimensions," Phys. Rev. Lett.

102, 233903 (2009).
34. S. Kumar and A. Hasegawa, "Quasi-soliton propagation in dispersion-managed optical fibers," Opt. Lett. **22**(6), 372–374 (1997).
35. A. Ankiewicz, D. J. Kedziora, and N. Akhmediev, "Rogue wave triplets," Phys. Lett. A **375**, 2782–2785 (2011).
36. A. Ankiewicz and N. Akhmediev, "Multi-rogue waves and triangular numbers," Rom. Rep. Phys. **69**, 104 (2017).
37. A. Chabchoub, N. Hoffmann, M. Onorato, and N. Akhmediev, "Super rogue waves: observation of a higher-order breather in water waves," Phys. Rev. X **2**, 011015 (2012).
38. F. Baronio, B. Frisquet, S. Chen, G. Millot, S. Wabnitz, and B. Kibler, "Observation of a group of dark rogue waves in a telecommunication optical fiber," Phys. Rev. A **97**, 013852 (2018).
39. N. Akhmediev, A. Ankiewicz, and J. M. Soto-Crespo, "Rogue waves and rational solutions of the nonlinear Schrödinger equation," Phys. Rev. E **80**, 026601 (2009).
40. S. Chen, J. M. Soto-Crespo, and Ph. Grelu, "Dark three-sister rogue waves in normally dispersive optical fibers with random birefringence," Opt. Express **22**(22), 27632–27642 (2014).
41. S. Chen, X.-M. Cai, Ph. Grelu, J. M. Soto-Crespo, S. Wabnitz, and F. Baronio, "Complementary optical rogue waves in parametric three-wave mixing," Opt. Express **24**(6), 5886–5895 (2016).
42. P. A. Clarkson and C. M. Cosgrove, "Painlevé analysis of the nonlinear Schrödinger family of equations," J. Phys. A Math. Gen. **20**, 2003–2024 (1987).
43. Y. Kodama and A. Hasegawa, "Nonlinear pulse propagation in a monomode dielectric guide," IEEE J. Quantum Electron. **QE-23**, 510–524 (1987).
44. G. P. Agrawal, *Nonlinear Fiber Optics*, 4th ed. (Academic, 2007).
45. F. Baronio, C. De Angelis, M. Marangoni, C. Manzoni, R. Ramponi, and G. Cerullo, "Spectral shift of femtosecond pulses in nonlinear quadratic PPSLT Crystals," Opt. Express **14**(11), 4774–4779 (2006).
46. J. Moses and F. W. Wise, "Controllable self-steepening of ultrashort pulses in quadratic nonlinear media," Phys. Rev. Lett. **97**, 073903 (2006).
47. J. Moses, B. A. Malomed, and F. W. Wise, "Self-steepening of ultrashort optical pulses without self-phase-modulation," Phys. Rev. A **76**, 021802(R) (2007).
48. M. Bache, O. Bang, B. B. Zhou, J. Moses, and F. W. Wise, "Optical Cherenkov radiation in ultrafast cascaded second-harmonic generation," Phys. Rev. A **82**, 063806 (2010).
49. A. Ankiewicz, D. J. Kedziora, A. Chowdury, U. Bandelow, and N. Akhmediev, "Infinite hierarchy of nonlinear Schrödinger equations and their solutions," Phys. Rev. E **93**, 012206 (2016).
50. H. H. Chen, Y. C. Lee, and C. S. Liu, "Integrability of nonlinear hamiltonian systems by inverse scattering method," Phys. Scr. **20**, 490–492 (1979).
51. D. J. Kaup and A. C. Newell, "An exact solution for a derivative nonlinear Schrödinger equation," J. Math. Phys. **19**, 798–801 (1978).
52. V. S. Gerdjikov and M. I. Ivanov, "The quadratic bundle of general form and the nonlinear evolution equations. Hierarchies of Hamiltonian structures," Bulg. J. Phys. **10**, 130–143 (1983).
53. A. Kundu, "Landau-Lifshitz and higher-order nonlinear systems gauge generated from nonlinear Schrödinger type equations," J. Math. Phys. **25**, 3433–3438 (1984).
54. W. Eckhaus, "The long-time behaviour for perturbed wave-equations and related problems," in *Trends in Applications of Pure Mathematics to Mechanics, Lecture Notes in Physics*, R. Kröner and K. Kirchgässner, eds. Vol 249, (Springer, 1986).
55. S. Xu and J. He, "The rogue wave and breather solution of the Gerdjikov-Ivanov equation," J. Math. Phys. **53**, 063507 (2012).
56. H. N. Chan, K. W. Chow, D. J. Kedziora, R. H. J. Grimshaw, and E. Ding, "Rogue wave modes for a derivative nonlinear Schrödinger model," Phys. Rev. E **89**, 032914 (2014).
57. J. He, S. Xu, and Y. Cheng, "The rational solutions of the mixed nonlinear Schrödinger equation," AIP Adv. **5**, 017105 (2015).
58. Zhaqilao, "On *N*th-order rogue wave solution to the generalized nonlinear Schrödinger equation," Phys. Lett. A **377**, 855–859 (2013).
59. S. Chen and D. Mihalache, "Vector rogue waves in the Manakov system: diversity and compossibility," J. Phys. A Math. Theor. **48**, 215202 (2015).
60. S. Chen, "Twisted rogue-wave pairs in the Sasa-Satsuma equation," Phys. Rev. E **88**, 023202 (2013).
61. S. Chen and L.-Y. Song, "Peregrine solitons and algebraic soliton pairs in Kerr media considering space-time correction," Phys. Lett. A **378**, 1228–1232 (2014).
62. F. Baronio, M. Conforti, A. Degasperis, S. Lombardo, M. Onorato, and S. Wabnitz, "Vector rogue waves and baseband modulation instability in the defocusing regime," Phys. Rev. Lett. **113**, 034101 (2014).
63. F. Baronio, S. Chen, Ph. Grelu, S. Wabnitz, and M. Conforti, "Baseband modulation instability as the origin of rogue waves," Phys. Rev. A **91**, 033804 (2015).
64. F. Baronio, S. Chen, and D. Mihalache, "Two-color walking Peregrine solitary waves," Opt. Lett. **42**(18), 3514–3517 (2017).
65. F. Baronio, "Akhemdiev breathers and Peregrine solitary waves in a quadratic medium," Opt. Lett. **42**(9), 1756–1759 (2017).